Solid State Communications 152 (2012) 1241–1243

Contents lists available at SciVerse ScienceDirect

Solid State Communications

journal homepage: www.elsevier.com/locate/ssc

Strong P-band emission and third harmonic generation from ZnO nanorods

J.I. Jang [a,*], S. Park [a], N.L. Frazer [b], J.B. Ketterson [b], S. Lee [c], B.K. Roy [c], J. Cho [c]

[a] Department of Physics, Applied Physics and Astronomy, Binghamton University, P.O. Box 6000, Binghamton, NY 13902, USA
[b] Department of Physics and Astronomy, Northwestern University, 2145 Sheridan Road, Evanston, IL 60208, USA
[c] Department of Mechanical Engineering & Materials Science and Engineering Program, Binghamton University, P.O. Box 6000, Binghamton, NY 13902, USA

ARTICLE INFO

Article history:
Received 6 January 2012
Received in revised form
12 March 2012
Accepted 12 April 2012
by D.J. Lockwood
Available online 24 April 2012

Keywords:
A. ZnO nanorods
D. Stimulated emission
D. Third harmonic generation

ABSTRACT

We report the room-temperature photoluminescence (PL) and broadband nonlinear optical (NLO) responses from high-quality ZnO nanorods grown by hydrothermal deposition. Based on the PL measurements, we find that the optical quality of ZnO nanorods critically depends on the packing and alignment of the rod structures. Our ZnO nanorods exhibit very strong third harmonic generation with suppressed second harmonic generation when the fundamental wavelength is varied in the range of 1060–2120 nm. Our results imply that ZnO nanostructures can potentially be utilized for various optoelectronic applications involving third-order NLO processes.

One-dimensional semiconducting nanorod and wire structures are potentially important for nanoscale electronic and photonic applications [1,2]. In particular, ZnO nanorods have attracted special interest in connection with high-efficiency optoelectronic applications working in a blue–UV regime at room temperature [2–4]. Renewed interest in ZnO-based nanostructures has recently been generated from the perspective of solar-cell applications and the relevant photovoltaic efficiency turns out to depend critically on having high crystallinity in the active medium [5]. The photoluminescence (PL) technique has been employed not only to investigate defect levels in ZnO [6], but also to demonstrate room-temperature stimulated emission in various ZnO nanostructures [2,7–9]. In addition, the nonlinear optical (NLO) properties of ZnO are also promising [10–18]. It is known that ZnO films exhibit strong second harmonic generation (SHG) through a large second-order susceptibility $\chi^{(2)}$ [10–13]. Also, the third-order NLO properties of ZnO films have been characterized using the Z-scan technique and third harmonic generation (THG), however only within a limited wavelength range [12–17]. Here, we report both PL and anomalous NLO responses obtained from hydrothermal-grown ZnO nanorods using a widely tunable pulsed laser.

Our ZnO nanorods were grown by hydrothermal deposition [19,20] at 90 °C on the surface of a seed layer, spin-coated on the fluorine-doped tin oxide (FTO)-coated glass substrate [21]. Two different precursors containing 750 mM (sample 1) and 50 mM (sample 2) of zinc acetate were employed to deposit the seed layers. The seed-layer condition is critical for the vertical growth of the *c*-axis oriented ZnO hexagonal nanorods since it contains crystallites that can promote the textured growth [22]. The thickness of both samples was about 1.5 μm. The microstructures of the as-deposited ZnO nanorods were characterized using a field-emission scanning electron microscope (SEM). Fig. 1 shows the SEM images of ZnO hexagonal nanorods from (a) sample 1 and (b) sample 2, respectively. Sample 1 yielded a more packed and aligned rod structure than sample 2 due to the larger number of nucleation sites. In contrast, the seed for sample 2 rendered a fewer number of nucleation sites, resulting in less alignment with disordered bundling. A higher degree of alignment for sample 1 was also confirmed by X-ray diffraction [21]. Also, the measured photovoltaic efficiencies are 2.3% (sample 1) and 1.2% (sample 2), respectively, which is consistent with Ref. [5].

In order to observe PL from the samples at room temperature, we employed one-photon band-to-band transitions using the frequency-tripled output of a mode-locked Nd:YAG laser (355 nm) with a pulse width of 30 ps and a repetition rate of 10 Hz. The corresponding excitation fluence P was varied from 0.2 mJ/cm^2 to 20 mJ/cm^2. The same laser was also used to pump an optical parametric amplifier (OPA) to generate idler pulses in the range of 1060–2120 nm. We monitored SHG and THG responses as a function of the incident wavelength λ at a fluence of $P=150$ mJ/cm^2; a low-pass filter was employed, thereby ensuring that only NLO signals are transmitted. The PL (NLO) signal was collected in a reflection (transmission) geometry from the samples and focused onto a fiber-optic bundle. The output of the fiber-optic bundle was coupled to the entrance slit of a Spex

---

[*] Corresponding author.
E-mail address: jjoon@binghamton.edu (J.I. Jang).

0038-1098/$ - see front matter © 2012 Elsevier Ltd. All rights reserved.
http://dx.doi.org/10.1016/j.ssc.2012.04.028

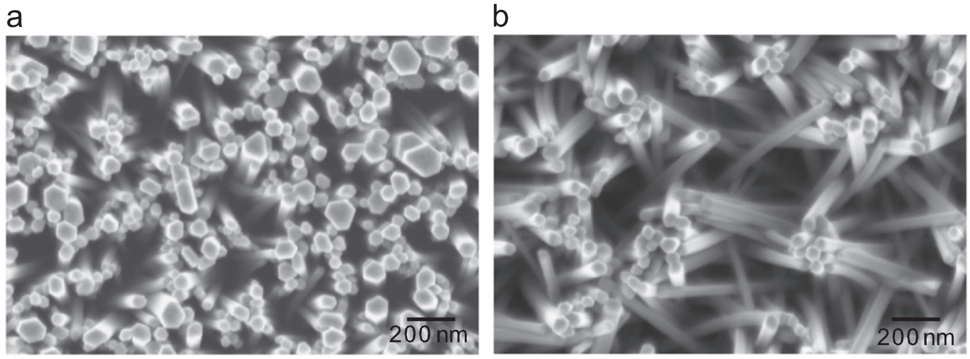

Fig. 1. Top-view SEM images of the ZnO nanorods grown from (a) sample 1 (750 mM seed layer) and (b) sample 2 (50 mM seed layer), respectively.

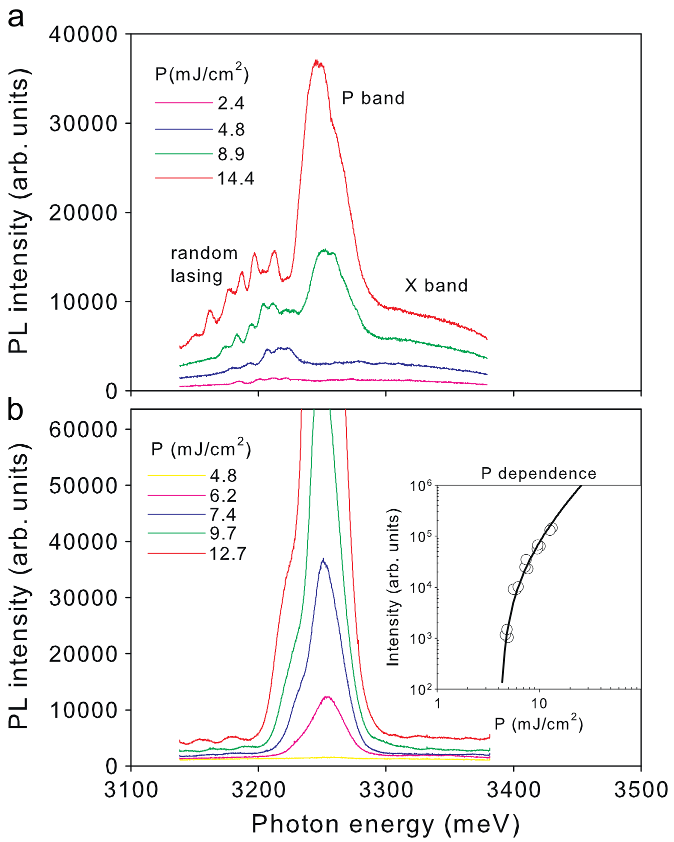

Fig. 2. (Color online) Time-integrated room-T PL spectra from (a) sample 2 for P=2.4–14.4 mJ/cm^2, showing a series of random lasing peaks and (b) sample 1 for P=4.8–12.7 mJ/cm^2. Inset: Power dependence of P-band intensities from sample 1.

500 M spectrometer and detected using a nitrogen-cooled Spectrum One CCD camera.

At the lowest excitation (P=0.2 mJ/cm^2), the PL band from both samples is broad and asymmetric [see the blue trace in Fig. 3(a)], arising from the radiative recombination of free excitons both directly and indirectly via emission of longitudinal optical phonons (X-band) [23]. On increasing the excitation level, the so-called P band appears and the emission intensity builds up superlinearly, indicating radiative recombination of photon-like excitons near the polariton bottleneck due to efficient exciton–exciton scattering [24]. Fig. 2(a) plots several PL spectra obtained from sample 2, when P is varied from 2.4 mJ/cm^2 to 14.4 mJ/cm^2, showing a series of sharp peaks in the range of 3150–3250 meV. This random lasing is typical of ZnO bulk, pellet, film, and nanocrystals with moderate impurity levels [8,25–27]. This indicates that sample 2 contains sufficient random scatterers, which presumably arise from a varying alignment and spacing of the nanorods, as further evidenced by the absence of random lasing from sample 1.

We plot the time-integrated PL spectra from sample 1 in Fig. 2(b) for P=4.8–12.7 mJ/cm^2. Note first that no random lasing is observed; the minor ripples around 3150–3200 meV at P=12.7 mJ/cm^2 arise from coherent interference of scattered light inside our detection system due to very strong P-band emission. Also, stimulated P-band emission occurs below 5.0 mJ/cm^2 and this P band quickly saturates our CCD camera for $P > 9.0$ mJ/cm^2. Since P-band emission arises from scattering of two thermal excitons, the process is proportional to the square of the exciton density and has a threshold behavior. The circles in the inset correspond to the measured P-band intensities from sample 1 as a function of P. The solid curve is an empirical fit to the data with the quadratic form $(P-P_c)^2$, yielding a critical fluence of $P_c = 4.1$ mJ/cm^2. The corresponding P_c of sample 2 at room temperature was found to be about 7.5 mJ/cm^2, indicating that the alignment of nanorods can play a significant role in reducing the threshold value of P_c. Together with no random lasing behavior, this may suggest that sample 1 has a better structural quality with minimal imperfection compared with sample 2 and other ZnO-based materials.

We now describe the wavelength-dependent second- and third-order NLO properties of samples 1 and 2 obtained at room temperature for $\lambda = 1060-2120$ nm; the corresponding SHG and THG wavelength ranges are $\lambda/2 = 530-1060$ nm and $\lambda/3 = 353.3-706.7$ nm, respectively. However, due to a limitation of our low-pass filter, only transmitted light with a wavelength less than 800 nm was available, and therefore, we could not monitor the SHG intensities with $\lambda/2 > 800$ nm. Our technique is quite unique in that previous works [3,10–13,15,16] involved fixed or limited wavelength sources: conventional Nd:YAG or Ti–Sapphire lasers. We confirmed that any NLO signal from the substrate is negligible in our experimental range.

The series of red traces in Fig. 3(a) shows the observed THG intensities from sample 1 as λ varies in our experimental range. The corresponding data collection time was 5 s. The blue trace denotes the PL spectrum under our lowest excitation. First, note that the THG signals plummet when $\lambda/3$ approaches the bandgap of ZnO (368 nm). This arises due to strong absorption of the THG light near the bandgap. However, it is interesting that the THG intensity at $\lambda/3 = 374.1$ nm (cyan peak) is noticeably stronger than other peaks near the bandgap. This wavelength corresponds to 3313 meV, which is very close to the free-exciton energy at room temperature [23]. Therefore, we attribute this enhancement of the THG signal to a resonance effect in which the energy denominator of the associated $\chi^{(3)}$ tensor is significantly reduced due to the existence of the free-exciton level. The green traces in

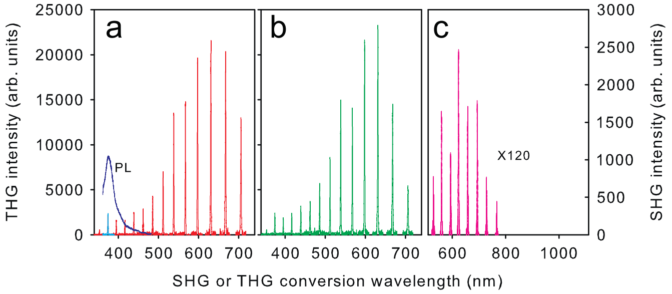

Fig. 3. (Color online) Wavelength-dependent THG responses from (a) sample 1 and (b) sample 2, respectively. (c) Corresponding SHG wavelength scan from sample 1.

Fig. 3(b) show the measured THG responses from sample 2 under the same conditions. The observed THG scan from sample 2 is very similar to that from sample 1 except for rather decreased THG signals around $\lambda/3 = 700$ nm; this is presumably caused by some deep impurity levels in sample 2 located at this wavelength. Based on essentially the same THG responses observed from samples 1 and 2, however, we believe that the third-order nonlinearity arises primarily from the bound electronic response of ZnO, with minimal dependence on the vertical alignment of the nanorod structures; but the diameter of nanorods could potentially affect THG responses. We plan to conduct wavelength-dependent Z-scan measurements and precisely determine the absolute value of $\chi^{(3)}$ in the range where strong THG responses occur without bandgap absorption.

The pink traces in Fig. 3(c) correspond to the SHG scan obtained from sample 1 under the same conditions for THG. Most interestingly, we found that the corresponding SHG signals from both samples are very small compared with the THG signals; note that the SHG intensities in Fig. 3(c) are scaled by a factor of 120. Considering the large value of $\chi^{(2)}$, about 14.3 pm/V [10,11], it is very surprising that the higher-order THG signals are several orders of magnitude stronger than the lower-order SHG counterpart. In fact, Wang et al. [11] observed a thickness-dependent $\chi^{(2)}$ in ZnO films, which is explained based on a model of stacking faults in the hexagonal ZnO lattices that presumably tend to cancel the overall SHG dipole moments for a micron-sized ZnO film. However, more studies should be conducted to confirm the model based on independent methods such as piezoelectric response, etc. Regardless of its microscopic origin, the strongly suppressed SHG can be viewed positively in that the third-order responses can then be exploited without the competition from SHG. In fact, ZnO has not been seriously considered for active optoelectronic applications involving third-order NLO processes. However, our results clearly suggest numerous third-order NLO applications working at near UV to mid-IR optical ranges, where the latter is especially important for stimulated Raman amplification and Kerr-effect-based all-optical switches in the mid-IR telecommunication [28].

In summary, we have conducted a series of optical measurements, including PL and wavelength-dependent NLO responses, on ZnO nanorods (samples 1 and 2) at room temperature. Based on the absence of random lasing and significantly lower P_c, also supported by the SEM image, we conclude that sample 1 has better optical and structural qualities for further optoelectronic and photovoltaic applications. Both samples exhibit very strong THG responses with suppressed SHG in our experimental range. Our results imply that ZnO nanostructures can be utilized for third-order NLO applications, without complications arising from second-order processes.

This work was supported by the National Science Foundation IGERT under Grant 0801685, the Northwestern Materials Research Center under NSF Grant DMR-0520513, and the Center for Autonomous Solar Power at Binghamton University under NASA Grant NNX09AT3OG.

References

[1] A.M. Morales, C.M. Lieber, Science 279 (1998) 208.
[2] M.H. Huang, S. Mao, H. Feick, H. Yan, Y. Wu, H. Kind, E.R. Rusoo, P. Yang, Science 292 (2001) 1897.
[3] X. Zhang, X. Zhang, J. Xu, X. Shan, J. Xu, D. Yu, Opt. Lett. 34 (2009) 2533.
[4] W.I. Park, J.S. Kim, G.-C. Yi, H.-J. Lee, Adv. Mater. 17 (2005) 1395.
[5] Y.M. Sun, J.H. Seo, C.J. Takacs, J. Seifter, A.J. Heeger, Adv. Mater. 23 (2011) 1679.
[6] W.I. Park, Y.H. Jun, S.W. Jung, G.-C. Yi, Appl. Phys. Lett. 82 (2003) 964.
[7] D.M. Bagnall, Y.F. Chen, Z. Zhu, T. Yao, S. Koyama, M.Y. Shen, T. Goto, Appl. Phys. Lett. 70 (1997) 2230.
[8] S.L. Cho, J. Ma, Y. Kim, Y. Sun, G.K.L. Wong, J.B. Ketterson, Appl. Phys. Lett. 75 (1999) 2761.
[9] C. Zhang, F. Zhang, X.W. Sun, Y. Yang, J. Wang, J. Xu, Opt. Lett. 34 (2009) 3349.
[10] G. Wang, G.K.L. Wong, J.B. Ketterson, Appl. Opt. 40 (2001) 5436.
[11] G. Wang, G.T. Keihne, G.K.L. Wong, J.B. Ketterson, X. Liu, R.P.H. Chang, Appl. Phys. Lett. 80 (2002) 401.
[12] B. Kulyk, Z. Essaidi, J. Luc, Z. Sofiani, G. Boudebs, B. Sahraoui, J. Appl. Phys. 102 (2007) 113113.
[13] B. Kulyk, Z. Essaidi, V. Kapustianyk, B. Turko, V. Rudyk, M. Partyka, M. Addou, B. Sahraoui, Opt. Commun. 281 (2008) 6107.
[14] H. Liao, W. Wen, G.K.L. Wong, G. Yang, Opt. Lett. 28 (2003) 1790.
[15] G.I. Petrov, V. Shcheslavskiy, V.V. Yakovlev, I. Ozerov, E. Chelnokov, V. Marine, Appl. Phys. Lett. 83 (2003) 3993.
[16] L. Guo, S. Yang, C. Yang, P. Yu, J. Wang, W. Ge, G.K.L. Wong, Appl. Phys. Lett. 76 (2000) 2901.
[17] M. Chattopadhyay, P. Kumbhakar, C.S. Tiwary, A.K. Mitra, U. Chatterjee, T. Kobayashi, Opt. Lett. 34 (2009) 3644.
[18] S. Mani, J.I. Jang, J.B. Ketterson, Appl. Phys. Lett. 93 (2008) 041902.
[19] Y.-H. Ni, X.-W. Wei, J.-M. Hong, Y. Yea, Mater. Sci. Eng. B 121 (2005) 42.
[20] Y. Sun, D.J. Riley, M.N.R. Ashfold, J. Phys. Chem. B 110 (2006) 15186.
[21] S. Lee, B. K. Roy, and J. Cho, unpublished.
[22] L.E. Greene, M. Law, D.H. Tan, M. Montano, J. Goldberger, G. Somorjai, P. Yang, Nano Lett. 5 (2005) 1231.
[23] W. Shan, W. Walukiewicz, J.W. Ager Jr., K.M. Yu, H.B. Yuan, H.P. Xin, G. Cantwell, Appl. Phys. Lett. 86 (2005) 191911.
[24] For *P*-band emission and alternative explanations, see C. Klingshirn, R. Hauschild, J. Fallert, H. Kalt, Phys. Rev. B **75** (2007) 115203.
[25] H. Cao, Y.G. Zhao, X. Liu, E.W. Seeling, R.P.H. Chang, Appl. Phys. Lett. 75 (1999) 1213.
[26] Y. Sun, G.K.L. Wong, J.B. Ketterson, Appl. Phys. Lett. 77 (2000) 2322.
[27] S.F. Yu, C. Yeun, S.P. Lau, W.I. Park, G.-C. Yi, Appl. Phys. Lett. 84 (2004) 3241.
[28] G.A. Thomas, D.A. Ackerman, P.R. Prucnal, S.L. Cooper, Phys. Today (2000) 30.